

Hepatic Blood Flow Measurements With Arterial and Portal Blood Flow Mapping in the Human Liver by Means of Xenon CT

Shigeru Sase, Morito Monden, Hiroshi Oka, Keizo Dono, Tatsuya Fukuta, and Iekedo Shibata

Purpose: The purpose of this work was to quantify arterial and portal blood flows in the human liver and to create blood flow maps by means of xenon CT.

Method: Mathematical procedures were developed based on a simplified model having two tissue components: liver tissue and portal organ tissue. Xe-CT studies were performed on 10 healthy volunteers (ages 33.4 ± 9.8 years), a patient with hepatocellular carcinoma (HCC), and a liver transplant recipient.

Results: Arterial and portal blood flows for the healthy subjects were 36.7 ± 5.2 and 65.2 ± 22.0 ml/100 ml/min. In the HCC patient, arterial blood flow was shown to be dominant in the tumoral area. From the results of the liver recipient, it was demonstrated that obtaining lambda values is important for proper evaluation of blood flows.

Conclusion: Xe-CT can provide substantial information on hepatic blood flow quantitatively and visually with separation of arterial and portal components.

Index Terms: Computed tomography—Xenon—Liver, blood flow.

INTRODUCTION

Quantitative mapping of regional arterial and portal blood flows in the human liver has not been achieved satisfactorily. Although mapping has been reported by perfusion measurements (1), the flow values obtained were significantly lower than commonly accepted ones. We tried to use the xenon CT method for this purpose (2) and have developed mathematical procedures based on the Fick principle. In this work, we present the results from healthy subjects and two specific cases.

THEORY

We describe two models for blood flow calculation in Xe-CT: One is for a single blood supply system for ordinary organs like the brain, and the other is for a dual blood supply system for the liver (3).

From Anzai Medical Co., Ltd. (S. Sase and T. Fukuta), Tokyo, Departments of Surgery and Clinical Oncology (M. Monden and K. Dono), Osaka University Medical School, Osaka, Moriguchi Keijinkai Hospital (H. Oka), Osaka, and Department of Neurosurgery (I. Shibata), Toho University School of Medicine, Tokyo, Japan. Address correspondence and reprint requests to S. Sase at Anzai Medical Co., Ltd., 3-9-15 Nishi-Shinagawa, Shinagawa-ku, Tokyo 141-0033, Japan. E-mail: sase@anzai-med.co.jp

Model for Single Blood Supply System (Single Supply Model)

In the case of a single blood supply system, the model in Fig. 1 is used for Xe-CT to calculate blood flow. Equation 1 is derived based on the Fick principle:

$$\frac{dC(t)}{dt} = f \cdot [C_a(t) - C_v(t)] \quad (1)$$

where $C(t)$, $C_a(t)$, and $C_v(t)$ are the time-dependent xenon concentrations in the tissue, arterial blood, and venous blood, respectively, and f is the blood flow per unit volume of the tissue. This equation means that the xenon concentration change rate in the tissue is the product of the blood flow and the xenon concentration difference between the entrance (arterial blood) and the exit (venous blood). The ratio of $C(t)$ to $C_v(t)$ is defined as λ_s , which is called the xenon solubility coefficient. With use of λ_s , Eq. 1 is described as

$$\frac{dC(t)}{dt} = f \cdot \left[C_a(t) - \frac{C(t)}{\lambda_s} \right] \quad (2)$$

This differential equation leads to the Kety-Schmidt equation (Eq. 3).

$$C(t) = f \cdot \int_0^t C_a(x) \cdot e^{-(f/\lambda_s)(t-x)} dx \quad (3)$$

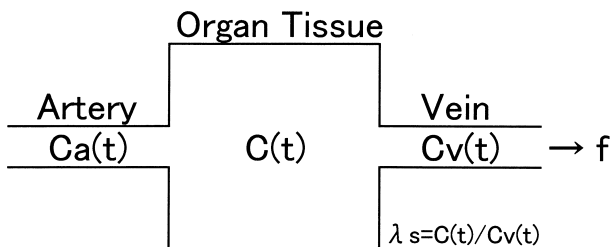


FIG. 1. Schema of the single supply model. $C(t)$, $C_a(t)$, and $C_v(t)$ represent time-dependent xenon concentrations in the organ tissue, arterial blood, and venous blood, respectively. Blood flow per unit volume of tissue is indicated by f .

where t is the time since the start of xenon inhalation. Equation 3 demonstrates that f and λ_s can be calculated by using two kinds of measured data: $C(t)$ and $C_a(t)$.

Model for Dual Blood Supply System (Dual Supply Model)

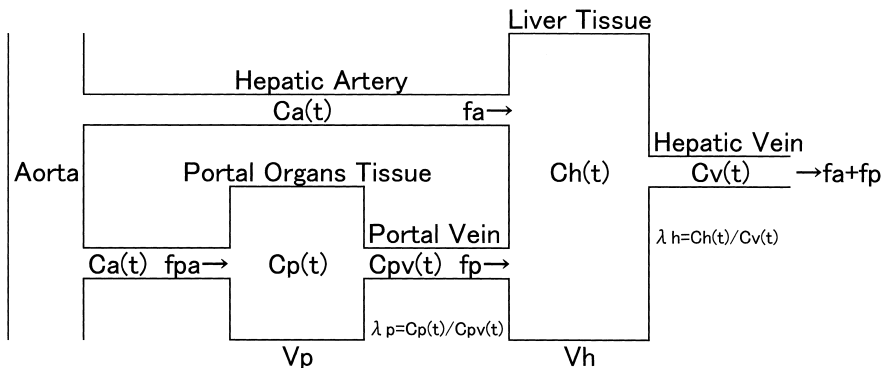
We used the model in Fig. 2 for the dual blood supply system for the liver to calculate hepatic blood flow by Xe-CT. Portal organs include the stomach, small intestine, large intestine, pancreas, gallbladder, and spleen. With respect to the liver tissue, Eq. 4 can be derived based on Eq. 1 considering two paths of blood flow: the hepatic artery–liver tissue–hepatic vein and the portal vein–liver tissue–hepatic vein:

$$\frac{dC_h(t)}{dt} = f_a \cdot [C_a(t) - C_v(t)] + f_p \cdot [C_{pv}(t) - C_v(t)] \quad (4)$$

where $C_h(t)$, $C_a(t)$, $C_v(t)$, and $C_{pv}(t)$ are the time-dependent xenon concentrations in the liver tissue, arterial blood, venous blood, and portal blood, respectively, and f_a and f_p are the arterial and portal blood flows per unit volume of the liver tissue, respectively. In respect to the portal organs tissue, Eq. 5 can be derived just like Eq. 1:

$$\frac{dC_p(t)}{dt} = f_{pa} \cdot [C_a(t) - C_{pv}(t)] \quad (5)$$

where $C_p(t)$ is the time-dependent xenon concentration in the portal organs tissue and f_{pa} is the blood flow per unit



volume of the portal organ tissue. The ratio of $C_h(t)$ to $C_v(t)$ and that of $C_p(t)$ to $C_{pv}(t)$ are defined as λ_h and λ_p , respectively; then Eqs. 4 and 5 become

$$\frac{dC_h(t)}{dt} = f_a \cdot \left[C_a(t) - \frac{C_h(t)}{\lambda_h} \right] + f_p \cdot \left[\frac{C_{pv}(t)}{\lambda_p} - \frac{C_h(t)}{\lambda_h} \right] \quad (6)$$

and

$$\frac{dC_p(t)}{dt} = f_{pa} \cdot \left[C_a(t) - \frac{C_p(t)}{\lambda_p} \right] \quad (7)$$

The differential equation (Eq. 7) can be solved as

$$C_p(t) = f_{pa} \cdot \int_0^t C_a(x) \cdot e^{-(f_{pa}/\lambda_p)(t-x)} dx \quad (8)$$

where t is the time since the start of xenon inhalation. Defining the volumes of the liver tissue and portal organ tissue as V_h and V_p , respectively, f_{pa} is equal to $V_h/V_p \cdot f_p$. Then Eq. 8 becomes

$$C_p(t) = \frac{V_h}{V_p} \cdot f_p \cdot \int_0^t C_a(x) \cdot e^{-(V_h/V_p)(f_p/\lambda_p)(t-x)} dx \quad (9)$$

Substituting Eq. 9 for Eq. 6, Eq. 6 becomes

$$\begin{aligned} \frac{dC_h(t)}{dt} &= f_a \cdot C_a(t) \\ &+ \frac{f_p^2}{\lambda_p'} \cdot \int_0^t C_a(x) \cdot e^{-(f_p/\lambda_p')(t-x)} dx \\ &- \frac{f_a + f_p}{\lambda_h} \cdot C_h(t) \end{aligned} \quad (10)$$

where λ_p' is $V_p/V_h \cdot \lambda_p$. This differential equation (Eq. 10) can be solved as

$$\begin{aligned} C_h(t) &= f_a \cdot \int_0^t C_a(y) \cdot e^{-(f_a + f_p)/\lambda_h(t-y)} dy \\ &+ \frac{f_p^2}{\lambda_p'} \cdot \int_0^t \left[\int_0^y C_a(x) \cdot e^{-(f_p/\lambda_p')(y-x)} dx \right] \cdot e^{-(f_a + f_p)/\lambda_h(t-y)} dy \end{aligned} \quad (11)$$

FIG. 2. Schema of the dual supply model. $C_h(t)$, $C_a(t)$, $C_v(t)$, and $C_{pv}(t)$ represent time-dependent xenon concentrations in the liver tissue, arterial blood, venous blood, and portal blood, respectively. Arterial and portal blood flows per unit volume of the liver tissue are indicated by f_a and f_p , respectively. $C_p(t)$ represents time-dependent xenon concentration in the portal organs tissue, and f_{pa} indicates blood flow per unit volume of the portal organs tissue.

Equation 11 demonstrates that f_a , f_p , λ_h , and λ_p' can be theoretically calculated by using two kinds of measured data: $C_h(t)$ and $C_a(t)$. However, it would be practically difficult to find the best combination of f_a , f_p , λ_h , and λ_p' based on the measured data by Xe-CT. We assumed λ_p' is equal to λ_h for simplification and described λ_p' and λ_h as λ_d . Then Eq. 11 becomes

$$C_h(t) = f_a \cdot \int_0^t C_a(y) \cdot e^{-(f_a + f_p)/\lambda_d](t-y)} dy \\ + \frac{f_p^2}{\lambda_d} \cdot \int_0^t \left[\int_0^y C_a(x) \cdot e^{-(f_p/\lambda_d)(y-x)} dx \right] \\ \cdot e^{-(f_a + f_p)/\lambda_d](t-y)} dy \quad (12)$$

This is the equation we used in this work to obtain the arterial blood flow (f_a), portal blood flow (f_p), and lambda (λ_d) values in the human liver on a pixel-by-pixel basis in Xe-CT.

Figure 3 shows the time course CT enhancement changes as theoretical simulation results. Graphs for five combinations of the arterial blood flow (f_a) and portal blood flow (f_p) (ml/100 ml/min) are presented: $f_p/f_a = 100/0$, $75/25$, $50/50$, $25/75$, and $0/100$.

METHODS

Subjects

Ten healthy volunteers (seven men, three women; aged 33.4 ± 9.8 years, mean \pm SD) underwent four level Xe-CT studies of the liver following informed consent. In these 10 subjects, absence of liver disease was documented with laboratory screening and ultrasonic study of the liver. Two patients were chosen for this study following informed consent: One was a 67-year-old man

with a large hepatocellular carcinoma (HCC), and the other was a 52-year-old woman with citrullinemia who underwent a liver transplant operation.

Data Acquisition

The CT scanner that was used was an Xvision/GX (Toshiba Corp., Tokyo, Japan); a 512×512 matrix and 10 mm slice thickness were used. Exposure factors were 120 kVp, 200 mA, and 1 s scans. The applied protocol was a 4 min washin/5 min washout (4). CT scanning was performed at 1 min intervals at the level of the liver. Each subject was guided to stop breathing at the time of end-expiration whenever scanning was done.

The AZ-725 (Anzai Medical Co.) was used as the xenon gas inhalation system, and the inhaled xenon concentration was 20 or 25%. The AZ-7000W (Anzai Medical Co.) was used to create maps for the arterial blood flow (f_a), portal blood flow (f_p), and lambda (λ_d) and to evaluate the f_a , f_p , and λ_d values.

Data Processing

In this work, end-tidal xenon concentration was used instead of arterial xenon concentration, and the time-dependent change in end-tidal xenon concentration was fitted with a monoexponential curve. Thus, the monoexponential function obtained was used as the time-dependent arterial xenon concentration.

A Xe-CT study generated 10 CT images (1 baseline and 9 enhancement images) for each level of the liver; 40 CT images were generated in total for four levels. The position of each enhancement image was adjusted manually by parallel translation to coincide with that of the

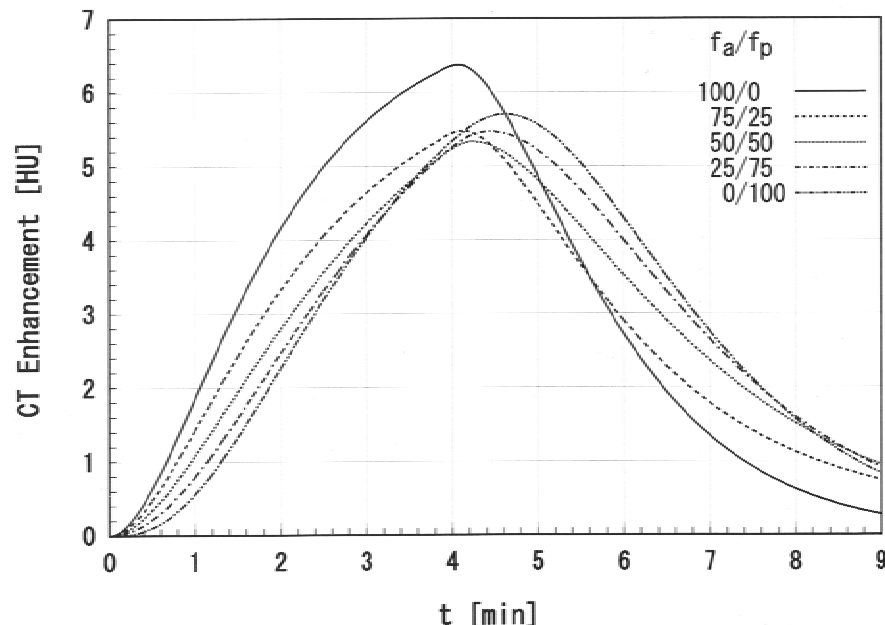


FIG. 3. Time course of CT enhancement changes as a result of theoretical simulation. Graphs for five combinations of arterial blood flow (f_a) and portal blood flow (f_p) (ml/100 ml/min) are presented, assuming lambda (λ_d [·]) is unity: $f_a/f_p = 100/0$, $75/25$, $50/50$, $25/75$, $0/100$. $C_a(t)$ was approximated with a monoexponential function: $C_a(t) = A_a \cdot (1 - e^{-K_a t})$ ($t \leq W$), $= C_a(W) \cdot e^{-K_a(t-W)}$ ($t > W$), where A_a , K_a , and W (washout timing) were assumed to be 7 HU, 1 min^{-1} , and 4 min, respectively.

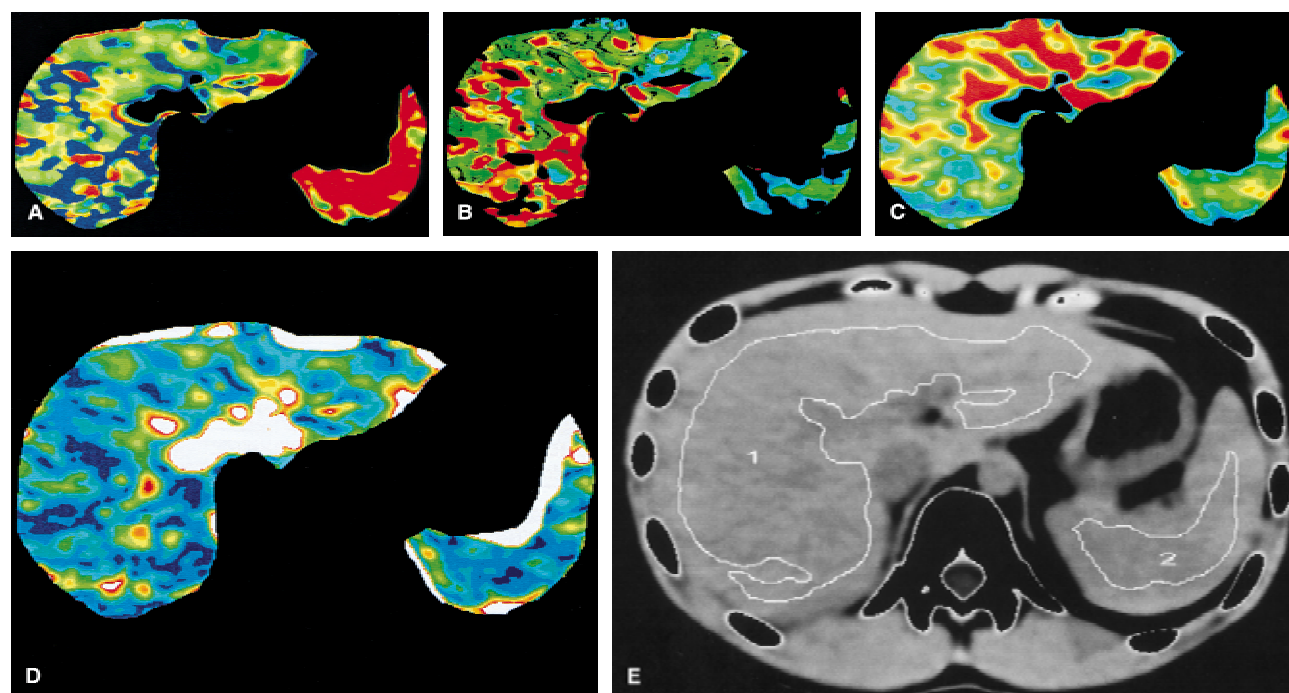


FIG. 4. A 20-year-old healthy man. **A:** Arterial blood flow map; **B:** portal blood flow map; **C:** lambda map; **D:** confidence map; **E:** baseline CT image with two regions of interest in the liver and spleen.

baseline image if necessary. We chose the most appropriate level for data processing out of four levels by visual inspection. Unweighted filtering over a 15×15 neighborhood was performed on the original CT images prior to computation.

We used the Gauss-Newton method to get the best combination of f_a , f_p , and λ_d values in Eq. 12 for each pixel within the liver and spleen. Let C_i ($i = 1, 2, \dots, n$) be the actual time course CT enhancement, and let C_{hi} ($i = 1, 2, \dots, n$) be the time course CT enhancement calculated from Eq. 12 with use of a certain combination of f_a , f_p , and λ_d values. The confidence value is defined as follows:

$$\text{confidence value} = \frac{\sum_{i=1}^n (C_i - C_{hi})^2}{n} (HU^2) \quad (13)$$

The best combination of f_a , f_p , and λ_d values makes the confidence value minimum and is the solution for Eq. 12. Thus obtained f_a , f_p , λ_d , and minimum confidence values were used to create the arterial blood flow map, portal blood flow map, lambda map, and confidence map, respectively. The confidence map shows how the theoretical change in time course CT enhancement led by the best combination of the f_a , f_p , and λ_d values can approxi-

TABLE 1. Hepatic and splenic blood flows (ml/100 ml/min) for healthy volunteers

Subject no.	Age (yrs)	Gender	Liver		Spleen	
			Arterial blood flow	Portal blood flow	Total blood flow	Arterial blood flow
1	36	Female	47.8	112.0	159.8	191.2
2	29	Female	31.8	60.7	92.5	149.2
3	20	Male	36.7	53.6	90.3	126.1
4	37	Male	37.7	79.9	116.8	^a
5	27	Male	33.5	68.8	102.4	135.1
6	23	Male	43.2	52.8	96.0	125.6
7	28	Male	37.1	86.7	123.8	163.9
8	42	Female	34.7	47.2	81.9	143.7
9	40	Male	31.7	48.1	79.8	^a
10	52	Male	33.2	41.6	74.8	118.1
Average ^b			36.7 ± 5.2	65.2 ± 22.0	101.8 ± 25.7	144.1 ± 24.1

^a Spleen did not exist in the selected level.

^b Data are presented as means ± SD.

TABLE 2. Lambda values of liver derived from single and dual supply models for healthy volunteers

Subject no.	Age (yrs)	Gender	Single supply model lambda (λ_s)	Dual supply model lambda (λ_d)	λ_d/λ_s
1	36	Female	1.07	1.05	0.98
2	29	Female	0.87	0.86	0.99
3	20	Male	0.89	0.91	1.02
4	37	Male	0.82	0.81	0.99
5	27	Male	1.11	1.11	1.00
6	23	Male	0.78	0.78	1.00
7	28	Male	0.97	0.96	0.99
8	42	Female	0.91	0.90	0.99
9	40	Male	0.80	0.82	1.03
10	52	Male	0.98	0.93	0.95
Average ^a			0.92 ± 0.11	0.91 ± 0.10	0.99 ± 0.02

^a Data are presented as means ± SD.

mate the actual change and can be used as the index of the reliability of the f_a , f_p , and λ_d values for each pixel. We set a threshold of the confidence value at 4 HU² in the confidence map. Whenever we drew a region of interest (ROI) on the liver for data evaluation, pixels having higher confidence values than the threshold were excluded from the ROI.

Comparison of Lambda Values Derived from Single and Dual Supply Models

When the single supply model is applied to the liver tissue, the derived blood flow values (the f values) will result in a systemic bias toward underestimation. However, the derived lambda values (the λ_s values) will be close to the true values of the xenon solubility coefficient. We calculated both the λ_s and the λ_d values of the liver tissue for each healthy subject and compared these two values to determine their relationship.

RESULTS AND DISCUSSION

Healthy Subjects

Figure 4 demonstrates the arterial blood flow map, portal blood flow map, lambda map, confidence map, and baseline CT image for the 20-year-old healthy man. The mapping for the spleen was performed and presented together with that for the liver. An ROI is shown on the liver in the baseline CT image (Fig. 4A). The mean arterial and portal blood flows in the ROI were 36.7 and

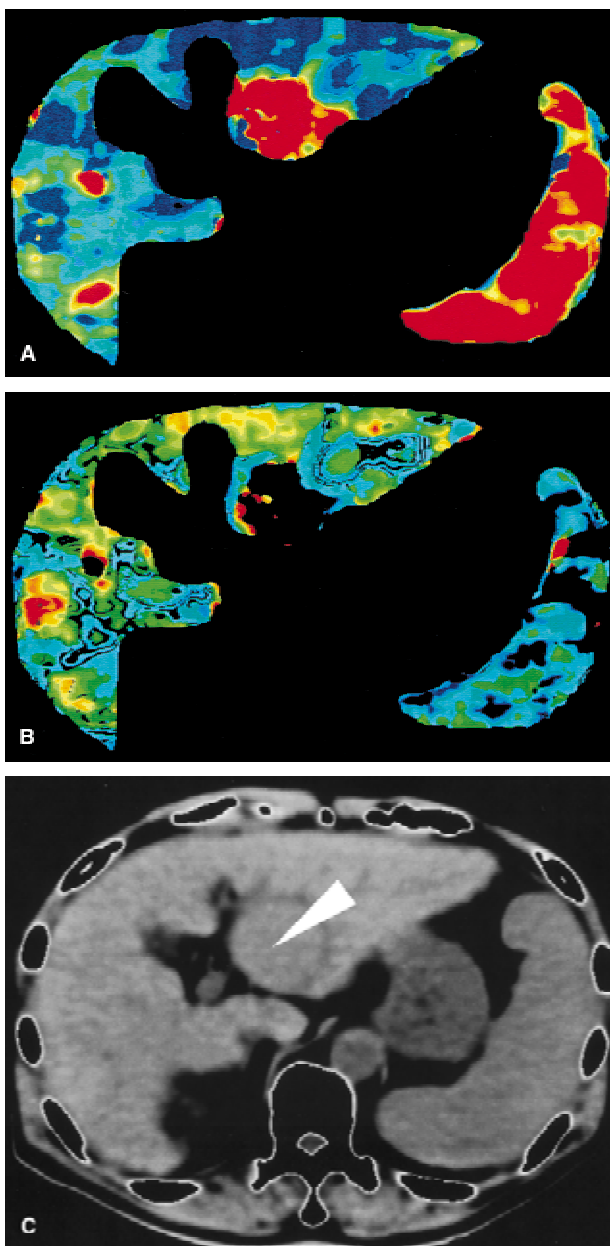


FIG. 5. A 67-year-old man with hepatocellular carcinoma. **A:** Arterial blood flow map; **B:** portal blood flow map; **C:** baseline CT image with an arrowhead at a large tumoral area.

53.6 ml/100 ml/min, respectively. In Table 1, the hepatic and splenic blood flow data for the 10 healthy subjects are listed. The average values for the arterial and portal blood flows of the liver were 36.7 and 65.2 ml/100 ml/min, respectively, which are consistent with the reported normative values measured by other methods (5–7). The average splenic blood flow was 144.1 ml/100 ml/min.

Table 2 shows the λ_s and λ_d values of the liver for each healthy subject. The ratio of λ_d to λ_s is also listed. It is noted that the λ_s and λ_d values were very close to each other for every subject; the average ratio of λ_d to λ_s was

TABLE 3. Hepatic and splenic blood flows (ml/100 ml/min) for a 67-year-old man with hepatocellular carcinoma

Organ	Arterial blood flow	Portal blood flow
Liver (large tumoral area)	114.3	4.9
Liver (remaining area)	18.4	32.4
Spleen	124.6	—

0.99 ± 0.02 (mean \pm SD). This suggests we can use the lambda map (λ_d map) to determine the xenon solubility coefficient of the liver tissue.

HCC Case

Figure 5 shows the arterial blood flow map, portal blood flow map, and baseline CT image for the 67-year-old man with HCC. The area of large HCC is indicated with an arrowhead in Fig. 5C. It is known that the HCC tissue usually receives only the arterial blood as a result of angiogenesis. This is clearly demonstrated in the arterial and portal blood flow maps (Fig. 5A and B). On the one hand, almost zero flow is shown in the large HCC area in the portal blood flow map. On the other, a remarkably high flow is shown in the same area in the arterial blood flow map. In Table 3, the blood flows for the tumoral area and the remaining area of the liver and the splenic blood flow are listed. The tumoral area is shown to receive a large blood supply (114.3 ml/100 ml/min) from the artery. It is noted that although the blood flow in the liver except the tumoral area is substantially lower than the normal range (Table 1), the

spleen is shown to have sufficient blood supply (124.6 ml/100 ml/min).

Liver Transplant Recipient

Figure 6 demonstrates the arterial blood flow map, portal blood flow map, lambda map, and baseline CT image for the 52-year-old woman, a liver transplant recipient. In Fig. 6D, the transplanted liver and recipient's own liver are shown with ROIs 1 and 2, respectively. It is characteristic that the lambda for the transplanted liver and that for recipient's own liver are quite different in Fig. 6C. The lambda value is considered to reflect the xenon solubility in the tissue; high solubility leads to large lambda. Since solubility is a kind of physical property of the tissue, liver tissue segments from different individuals are likely to have different lambda values. Figure 6C demonstrates the case that the lambda values of the liver tissue from two individuals are quite different. In Fig. 7, the arterial and portal blood flow maps are shown, assuming the lambda value of the entire tissue is unity. The blood flow maps change drastically from Fig. 6 to Fig. 7 as a result of the change in lambda handling.

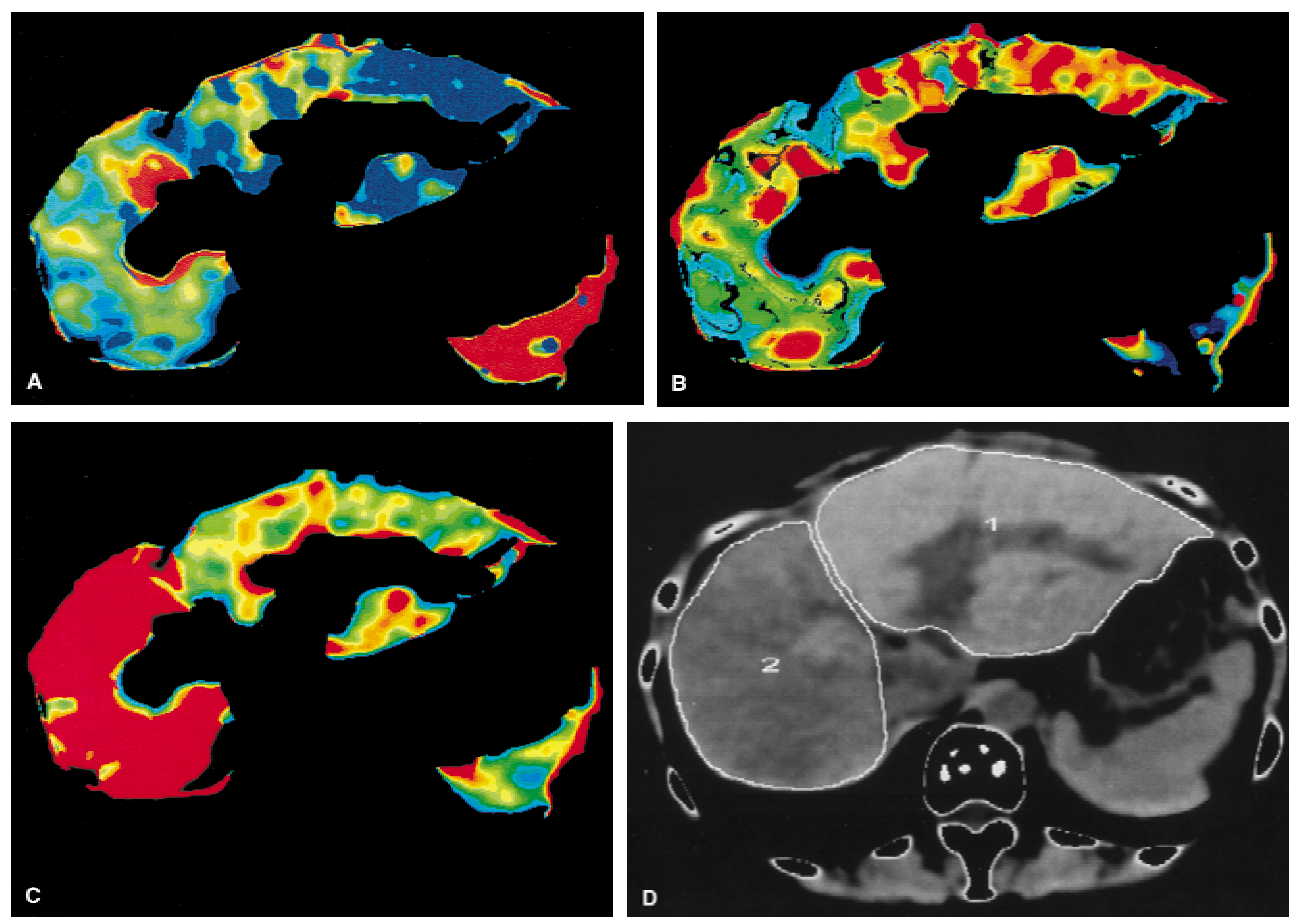


FIG. 6. A 52-year-old woman (liver transplant recipient). **A:** Arterial blood flow map; **B:** portal blood flow map; **C:** lambda map; **D:** baseline CT image with regions of interest 1 and 2 indicating transplanted liver and recipient's own liver, respectively.

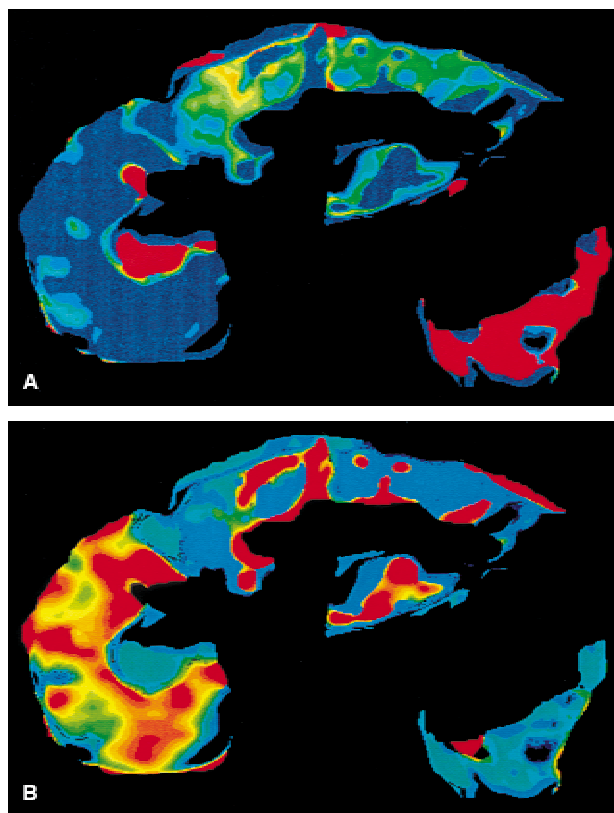


FIG. 7. Blood flow maps for a 52-year-old woman (the same subject as in Fig. 6), assuming lambda is unity in the entire tissue. **A:** Arterial blood flow map; **B:** portal blood flow map.

Table 4 shows the arterial blood flow, portal blood flow, and lambda values obtained from the data in Figs. 6 and 7. It is clearly understood from Figs. 6 and 7 and Table 4 that lambda should be calculated precisely for each pixel to obtain correct values of the arterial and portal blood flows of the liver tissue.

CONCLUSIONS

Xe-CT could provide substantial information on hepatic blood flow quantitatively and visually with separation of arterial and portal components. We summarize the major advantages of hepatic blood flow measurements by Xe-CT as follows:

1. Quantitative measurements of the arterial blood flow, portal blood flow, and lambda values can be obtained.
2. Noninvasive examination with use of end-tidal xenon as a substitute for arterial xenon can be performed.
3. Blood flow and lambda maps having the same shape and size as the CT image are created. This makes it possible to place ROIs based on the CT image, which has excellent quality anatomic information.

TABLE 4. Hepatic and splenic blood flows (ml/100 ml/min) and lambda for a 52-year-old woman (liver transplant recipient), calculated under two conditions: lambda variable and fixed

Organ	Lambda variable ^a	Lambda fixed ^b
Transplanted liver		
Arterial blood flow	19.5	26.9
Portal blood flow	65.6	34.5
Lambda	0.80	1.00
Recipient's own liver		
Arterial blood flow	33.8	2.9
Portal blood flow	37.8	68.4
Lambda	2.18	1.00
Spleen		
Arterial blood flow	155.3	159.2
Lambda	0.68	1.00

^a Lambda (λ_d) was calculated for each pixel (Fig. 6).

^b Lambda (λ_d) was assumed to be unity for every pixel (Fig. 7).

4. Multiple level measurements are possible with repeated moving of the CT table.
5. Repeat study is possible after a brief interval because inert xenon is nearly eliminated from the body within 15–20 min after the patient resumes breathing room air (washout).

The movement of the liver in accordance with respiration causes difficulty in this technique in obtaining high quality blood flow images. In this work, the subjects were guided by voice to stop breathing at the time of end-expiration. If respiration-gated automatic scanning were introduced, the burden of the patient could be alleviated and the examination itself could be simplified. We believe the hepatic blood flow measurements by Xe-CT could play a major role in determining the circulation state of the liver as a routine examination.

REFERENCES

1. Miles KA, Hayball MP, Dixon AK. Functional images of hepatic perfusion obtained with dynamic CT. *Radiology* 1993;188:405–11.
2. Gur D, Good WF, Herbert DL, et al. Blood flow mapping in the human liver by the xenon/CT method. *J Comput Assist Tomogr* 1985;9:447–50.
3. Taniguchi H, Oguro A, Koyama H, et al. Analysis of models for quantification of arterial and portal blood flow in the human liver using PET. *J Comput Assist Tomogr* 1996;20:135–44.
4. Kalender WA, Polacin A, Eidloch H, et al. Brain perfusion studies by xenon-enhanced CT using washin/washout study protocols. *J Comput Assist Tomogr* 1991;15:816–22.
5. Greenway CV, Stark RD. Hepatic vascular bed. *Physiol Rev* 1971; 51:23–65.
6. Sarper R, Fajman WA, Rypins EB, et al. A noninvasive method for measuring portal venous/total hepatic blood flow by hepatosplenic radionuclide angiography. *Radiology* 1981;141:179–84.
7. Mathie RT. Hepatic blood flow measurement with inert gas clearance. *J Surg Res* 1986;41:92–110.